Journal of The Electrochemical Society

Performances of Solid Oxide Cells with $La_{0.97}Ni_{0.5}Co_{0.5}O_{3-\delta}$ as Air-Electrodes

Journal of The Electrochemical Society, 2020 **167** 084522

Performances of Solid Oxide Cells with $La_{0.97}Ni_{0.5}Co_{0.5}O_{3-\delta}$ as Air-Electrodes

Qianli Ma,[1,=,z] Sebastian Dierickx,[2,=] Vaibhav Vibhu,[1] Doris Sebold,[1] Lambertus G. J. de Haart,[1] André Weber,[2,*] Olivier Guillon,[1,3] and Norbert H. Menzler[1,*]

[1] *Forschungszentrum Jülich GmbH, Institute of Energy and Climate Research (IEK), D-52425 Jülich, Germany*
[2] *Institute for Applied Materials (IAM-WET), Karlsruhe Institute of Technology (KIT), D-76131 Karlsruhe, Germany*
[3] *Jülich Aachen Research Alliance, JARA-Energy, D-52425 Jülich, Germany*

Based on previous studies of perovskites in the quasi-ternary system $LaFeO_3$–$LaCoO_3$–$LaNiO_3$, $La_{0.97}Ni_{0.5}Co_{0.5}O_3$ (LNC) is chosen as the most promising air-electrode material in the series for solid oxide cells (SOCs). The properties of the material itself have been investigated in detail. However, the evaluation of LNC97 air electrodes in practical SOCs is still at a very early stage. In the present study, SOCs were prepared based on LNC97 air electrodes. The I-U performance of the SOCs in both solid oxide fuel cell (SOFC) and solid oxide electrolysis cell (SOEC) modes, i.e. reversible SOCs (r-SOCs), was investigated systematically for different air-electrode designs, temperatures and fuel gases. In general, the performance of the r-SOCs tested in the present study is higher than the published results of other $LaFeO_3$–$LaCoO_3$–$LaNiO_3$-based SOCs and is comparable to or even better than state-of-the-art $La_{1-x}Sr_xFe_{1-y}Co_yO_3$ (LSCF)-based SOCs. Mid-term operation of about 1000 h for SOCs in both SOFC and SOEC modes primarily proved the stability of LNC97-based air electrodes. Impedance spectra were systematically applied to understand the polarization processes of the SOCs.

 [DOI: 10.1149/1945-7111/ab91cc]

Manuscript submitted March 2, 2020; revised manuscript received May 7, 2020. Published May 25, 2020.

Utilizing renewable energy sources such as solar and wind combined with stationary energy-storage systems is in all probability the ultimate solution to address increasing environmental concerns and a possible future lack of resources for fossil energy. However, solar and wind fluctuate and are not reliable power sources, which gives rise to significant challenges for operators of the existing electric grid. Auxiliary systems are needed to store excess power and re-generate it for peak electricity demand. Solid oxide cells (SOCs) can either generate electrical power using a broad range of fuels in solid oxide fuel cell (SOFC) mode or convert renewable electricity into the chemical energy of fuels in solid oxide electrolysis cell (SOEC) mode.[1] Such reversible applications make SOCs (r-SOCs) a possible auxiliary system for renewable energy sources. Compared to other kinds of power generators or electrolysis, SOCs possess high conversion efficiencies which can hardly be reached by any other system. The state-of-the-art $La_{1-x}Sr_xFe_{1-y}Co_yO_3$ (LSCF) and $La_{1-x}Sr_xCoO_3$ (LSC), although quite mature materials for air electrodes in SOC development, have long suffered from chemical and thermal expansion mismatch with the electrolyte material of 8 mol% Y_2O_3-stabilized ZrO_2 (8YSZ),[2,3] and with the metallic interconnects of SOC stacks.[4] The continuous depletion of strontium during their operation in SOCs causes the mismatches,[1,5] which is an intrinsic property of the materials and can hardly be avoided. Therefore, extensive attention has been paid in recent years to alternative Sr-free air-electrode materials. Among the possible candidates, the quasi-ternary system of $LaCoO_3$–$LaNiO_3$–$LaFeO_3$ shows good electrochemical performance,[6–8] high physical[7,9] and chemical stability[8,10] with other component of SOCs and is considered to provide promising candidates as alternatives to LSCF or LSC. A number of publications have already discussed the air-electrode performance of the $LaNi_xCo_yFe_{1-x-y}O_3$ system with symmetric cells or full cells.[6,8,11–15] Most of these studies report quite promising laboratory scale results. However, there has still been no discussion of the performance of SOCs close to practical application.

In previous studies, we overviewed the quasi-ternary system of $LaFeO_3$–$LaCoO_3$–$LaNiO_3$ considering the variation of electrical conductivity, oxygen permeation, oxygen surface exchange, thermal-expansion coefficient etc.[7] Of all the compositions, $La_{0.97}Ni_{0.5}Co_{0.5}O_3$ (LNC97) is selected as the best candidate when all of the above conditions are considered. A qualified air-electrode material should have high electronic conductivity, high ionic conductivity and high catalytic activity for the oxygen reduction reaction to achieve good air-electrode performance. LNC97 has been systematically discussed in an earlier publication involving all the possible conditions mentioned above with symmetric cells.[8] It is known that LNC97 has competitive electronic conductivity but relatively low oxide-ionic conductivity and catalytic activity in comparison to the state-of-the-art LSCF. Nevertheless, the latter two can be effectively improved by nano-infiltration of $Gd_{0.2}Ce_{0.8}O_{2-\delta}$ (GDC) enabling it to fit the criterion.[8] In addition, LNC97 also has much lower chemical reactivity with 8YSZ compared to that of state-of-the-art LSCF.[8] However, research on LNC97-based SOC full cells is still at quite an early stage and the evaluation of LNC97 at a practical application level is not clear.

In the current study, SOCs with dimensions of 5 cm × 5 cm were prepared based on LNC97 as the air-electrode material. I-U performance was investigated in detail in both solid oxide fuel cell (SOFC) and solid oxide electrolysis cell (SOEC) modes. Mid-term performance was also observed in SOFC and SOEC modes in the time range of about 1000 h. An impedance spectrum was applied to analyze the contribution of different cell components. The potential of LNC97-based SOCs in practical applications was discussed.

Experimental

Cell fabrication.—SOC half cells have been available commercially from CeramTech® and contain a NiO-8YSZ fuel-electrode support and functional layer, and a dense 8YSZ layer with dimensions of 5 cm × 5 cm × 0.5 mm. A dense GDC protective layer (thickness 0.5 μm) was applied on the half cells by magnetron sputtering; more details are provided in Refs. 2, 3 Powders of $La_{0.97}Ni_{0.5}Co_{0.5}O_3$ (LNC97) were prepared by Pechni's method[16] using nitrate solutions of La, Ni and Co in the corresponding cation ratios. Screen-printing pastes of LNC97 were prepared by mixing the solid powders with terpineol and ethyl cellulose. LNC97 was fabricated on the GDC protective layer by screen printing followed by heat treatment at 1100 °C. LNC97 layers were immersed in (Ce.Gd) nitrate solutions in vacuum and subsequently heated to 500 °C to achieve a loading of

[=] These authors contributed equally to this work.
[*] Electrochemical Society Member.
[z] E-mail: q.ma@fz-juelich.de

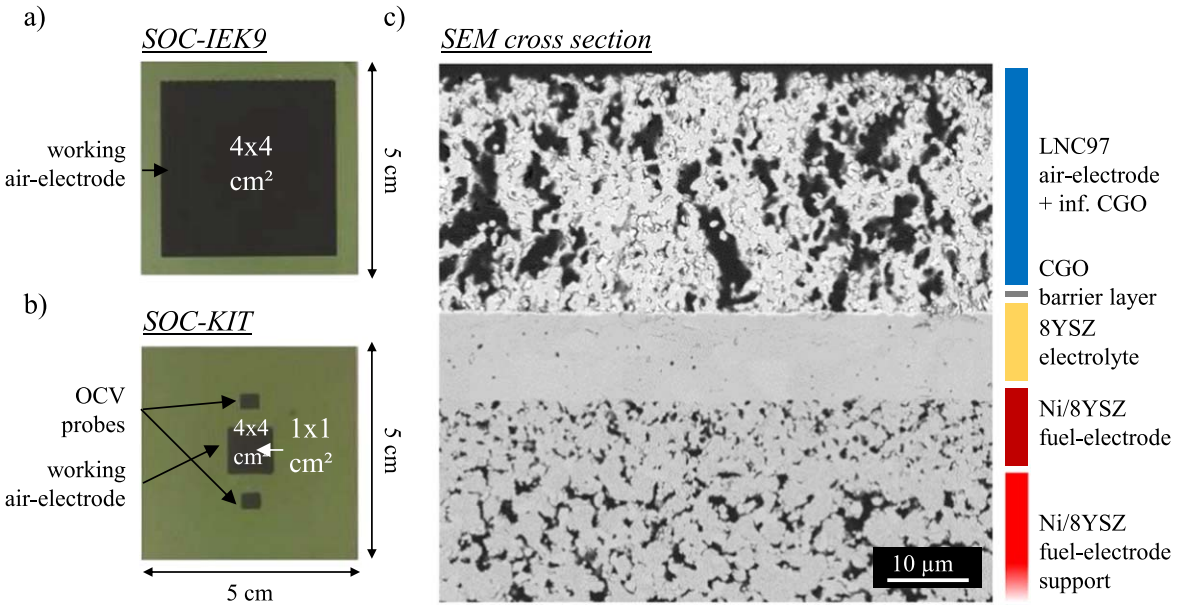

Figure 1. Images of SOCs tested in (a) Forschungszentrum Jülich, IEK-9 (SOC-IEK9) and (b) in Karlsruhe Institute of Technology (SOC-KIT). (c) SEM image of a cross section of the fabricated SOC.

8 wt% GDC (compared to LNC97). More specifics can be found in Ref. 8.

Single-cell geometry and microstructure.—The SOCs tested in the present work applied commercial half cells from CeramTec®, which have dimensions of 5 cm × 5 cm, and contain a fuel-electrode support, a fuel-electrode functional layer and dense 8YSZ layer, as shown in Table I. Two different air-electrode dimensions were applied for performance and durability testing. One has a 4 cm × 4 cm LNC97-based air electrode (SOC-IEK9), while the other has a 1 cm × 1 cm working electrode and two 0.4 cm × 0.3 cm OCV monitoring electrodes (SOC-KIT), as shown in Figs. 1a and 1b. SOC-IEK9 and SOC-KIT are identical except for the dimensions of the air electrodes.

Figure 1c shows the structure of a typical SOC in the present work obtained by scanning electron microscopy (SEM). From bottom to top, in accordance with Table I, the SOCs are composed of a commercial half-cell from CeramTec®, a dense GDC barrier layer, and an LNC97 air-electrode layer infiltrated by ∼8 wt% GDC inside LNC97 backbone. The function of GDC barrier layer is to prevent the possible reaction between LNC97 and 8YSZ. It has been confirmed that LNC97 and YSZ react at >1000 °C as powders. The main product is $La_2Zr_2O_7$.[8] This powder-based result shows that there is a kinetically driven tendency for both materials to react. Although the reaction between bulk LNC97 and bulk YSZ is not detectable by SEM with energy-dispersive X-ray spectroscopy (EDX), the performance of LNC97/8YSZ/LNC97 symmetric cells are slightly lower than that of LNC97/GDC/LNC97 symmetric cells,[8] which may be caused by higher conductivity of GDC compared to 8YSZ, or by slight reaction between LNC97 and 8YSZ which is not detectable by SEM-EDX. Nevertheless, to benchmark the state-of-the-art LSCF based SOCs, GDC barrier layers are still applied between LNC97 and 8YSZ layers although their reaction is much milder compared to those between LSCF and 8YSZ.[8] The function of the infiltrated GDC into LNC97 is to increase the oxide-ionic conductivity and catalytic activity of the air-electrode layer. The air-electrode and fuel-electrode (support) both have porosity of ∼30%, which fits the requirement of gas transportation during operation. 8YSZ and GDC layer are both quite dense, which can safely separate the air and fuel atmosphere. The contact between all the layers is realistic, which is the precondition of the satisfactory performances of the SOCs.

Cell testing.—The electrochemical characterization of both SOC types was performed in an alumina test housing placed inside a furnace. For electrical contacts, Ni and Pt or Au meshes (Pt: SOC-IEK9)/Au: SOC-KIT) were used at the anode and cathode side, respectively. Sealing between the gas compartments was implemented by a gold ring. Gas flow rates on the anode and cathode were controlled by mass flow controllers for both SOC types. The large SOC-IEK9 cells were primarily used for performance evaluation via current-voltage characteristics, whereas the SOC-KIT cells were additionally employed for a detailed electrochemical characterization via impedance spectroscopy.

SOC-IEK9.—During cell characterization in SOFC mode, the anode was flushed with 12% humidified hydrogen at a flow rate of 1 l min^{-1} and the cathode side with 2 l min^{-1} of dry air. During cell characterization in r-SOC mode, the anode was flushed with 50% humidified hydrogen at a flow rate of 1 l min^{-1} and the cathode side with 2 l min^{-1} of dry air. The current-voltage characteristics were measured with increasing current load by a sequential step change of 62.5 mA cm^{-2}, starting from zero until the voltage dropped below 0.6 V.

SOC-KIT.—The SOC-KIT cells were operated with synthetic air (79% N_2 and 21% O_2) at the cathode and humidified hydrogen at the anode. Fuel humidification was varied in a range between 5.5% and

Table I. Material composition and layer thicknesses of the tested SOC type.

Fuel-electrode support	Fuel-electrode	Electrolyte	Barrier layer	Air-electrode
Ni/8YSZ	Ni/8YSZ	8YSZ	GDC	LNC97 + inf. ∼8 wt% GDC
∼500 μm	∼7 μm	∼10 μm	∼0.5 μm	∼25 μm-

50%. The total gas flow rates for anode and cathode were maintained at a constant value of 0.25 l min^{-1} for all experiments. Impedance spectra were recorded under OCV conditions and under polarization (±1 A cm^{-2}) with a Solartron 1260 in a frequency range from 100 mHz to 1 MHz. Data quality was verified by applying the Kramers-Kronig test.[17] Evaluation of the impedance data was assisted by calculating the distribution of the relaxation times (DRT).[18,19]

Results and Discussion

I-U performance in SOFC mode.—Figure 2 shows the performance of SOCs in SOFC mode. In their function as a kind of power generator, SOFCs normally operate under fuel gas together with steam. Although H_2O itself is not a power source, the significance of the existence of H_2O in fuel gas is that H_2O has a catalytic impact on the fuel-electrode processes.[20–22] In all the SOCs tested in the present study, the only air-electrode gas applied is air. As mentioned above, two air-electrode designs were applied in the present study, SOC-IEK9 and SOC-KIT. The former design is closer to practical applications and has been tested at Forschungszentrum Jülich, where an evaluation of 16 cm^2 cells (Fig. 1a) is always performed before scaling up a novel material or design to stack level, and the performance of which can generally predict the situation of the cells in a real stack. The latter cell type with a 1 cm^2 active electrode area (Fig. 1b) is designed for detailed electrochemical characterization at Karlsruhe Institute of Technology.[23,24] The smaller active electrode area avoids lateral gradients and thus provides more details about the electrochemical processes determining cell performance. Typical I-U behavior of SOC-IEK9 at 800 °C is shown in Fig. 2a. The open-circuit voltage (OCV) of the cell is 0.99 V (with 12% H_2O in fuel gas), which fits well with the theoretical value, indicating the satisfactory gas tightness of the 8YSZ electrolyte and the sealing of the cell. At 0.7 V, the output current density is 2.0 A cm^{-2} (with 12% H_2O in fuel gas), which is among the best published performances for the state-of-the-art LSCF-based cells of similar construction and dimensions.[2,3,25,26] It should be mentioned that the commercial requirement for SOFC single-cell power output is >1.0 W cm^{-2}. Although the dimensions of SOC-IEK9 are still smaller than the normal commercial criterion (>10 cm × 10 cm), the scaling-up of SOC-IEK9 will not normally cause much performance loss. Since the performance of SOC-IEK9 is already much higher than the commercial level, it can be concluded that, judging merely from the power output, LNC97-based air electrodes present no difficulty for commercialization.

When the SOC-KIT design is applied, the performance is even higher. The open-circuit voltage (OCV) of the cell is 1.07 V (with 5.5% H_2O in fuel gas). The current density at 0.7 V is not testable because of the limited testing range of the current. However, lineal simulation of the I-U behavior shows the current density of 3.3 A cm^{-2} at 0.7 V. As a general point, in SOC testing, lab-level performance seems to be always higher than that of the level of scaling-up. The present study also shows a typical example. In the current case, the higher performance of SOC-KIT is related to the fuel and oxidant utilization (f.u. of 5.9% (5% H_2O) and 11.2% (50% H_2O)/o.u. 13.2% at 2 A cm^{-2}), which are set to be low in order to minimize lateral gradients in gas composition. Furthermore, the current was limited to 2 A, which additionally minimizes self-heating effects and related thermal gradients. A second reason for the performance difference is related to the contacting. In the case of air-electrode in dimension of 1 cm^2, in-plane ohmic losses in the current collector can be neglected. Furthermore, the setup contains mechanically decoupled flow fields that enable a well-defined and constant contact pressure between the contact grid and electrode. However, the area difference of the working air electrode is important. For the KIT design the fuel consumption only results in a negligible gradient along the electrodes, but for larger active areas as in the IEK9 design such gradients exist, which results in higher electrochemically activated areas at the gas entry side and lower ones at the outlet side.

The performance of SOFCs under 50% H_2O–50% H_2 fuel gas was also investigated. Although with respect to the power output fuel gas with such a high steam content is not suitable, such fuel gas is significant for r-SOCs, where the function of both the SOFC and SOEC can fulfilled. A relatively stable fuel gas supply is important for the longevity of the SOC system. Under higher steam content, the performance of both SOC-IEK9 and SOC-KIT decreased compared to their low-steam operation. However, SOC-IEK9 and SOC-KIT still show current densities of 1.7 A cm^{-2} and 2.3 A cm^{-2} (Figs. 2a and 2b) at 0.7 V and 800 °C, respectively. The performance of SOFCs under 50% H_2O–50% H_2 fuel gas has received less attention compared to that of low-steam fuels. According to the published results,[27–29] the above performances is also among the highest published data for the state-of-the-art LSCF based SOFCs.

The impedance spectra and the corresponding DRTs of SOC-KIT under OCV are shown in Fig. 3. Although the Nyquist plot can only distinguish the ohmic resistance and electrode resistance in ASR (Fig. 3a), DRT analysis gives much more information. As can be clearly seen from the DRT (Fig. 3b), the steam content strongly affects the low and high frequency part of the impedance, whereas the ohmic resistance (cross section with the real axis) and the cathode polarization (100–1000 Hz) remain unaffected. From previous studies on cells using the same fuel electrode, these two processes can be assigned to the gas diffusion in the fuel electrode support (10–100 Hz),[23,30] and the fuel electrode electrochemistry

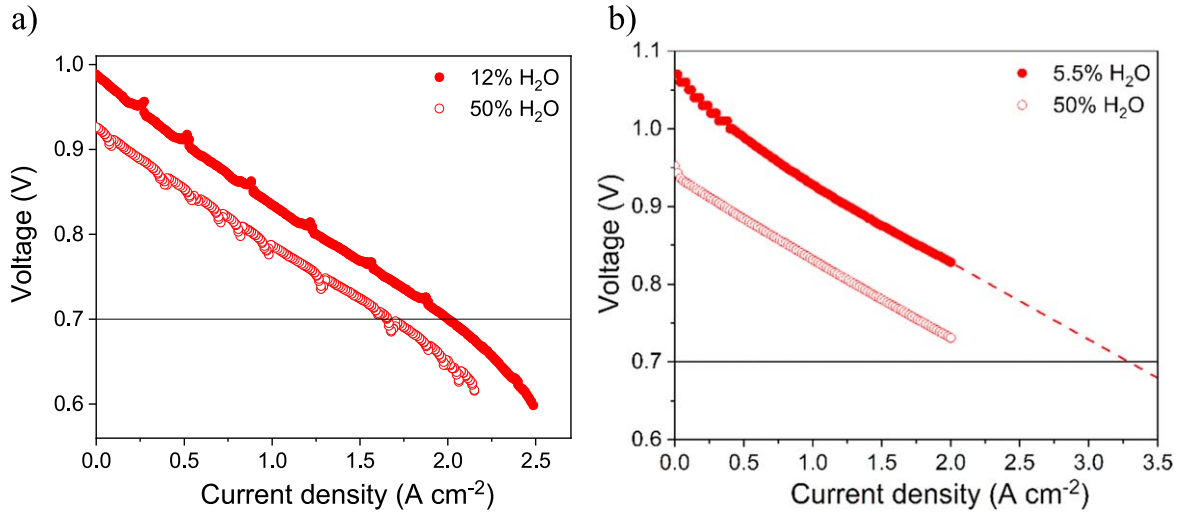

Figure 2. Current–voltage investigations of (a) SOC-IEK9 and (b) SOC-KIT at 800 °C in SOFC mode with different H_2O content in H_2O–H_2 fuel gases.

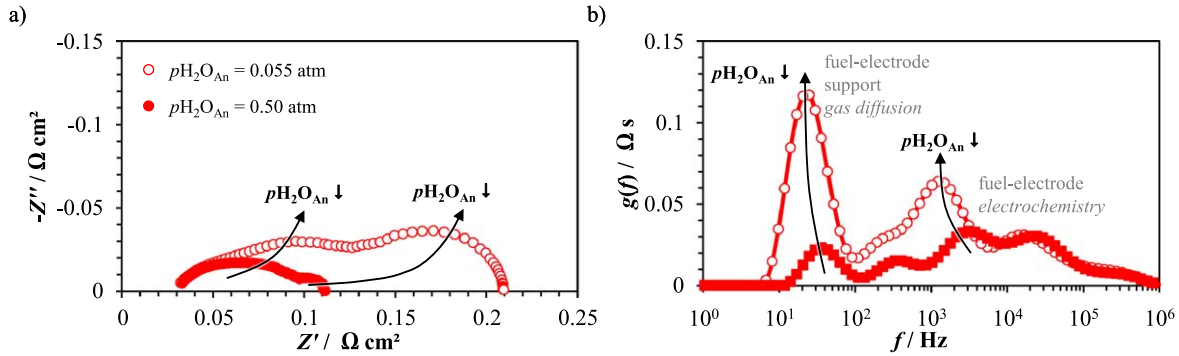

Figure 3. (a) Measured impedance spectra and (b) the calculated DRTs for 5.5% and 50% humidified hydrogen as fuel (corresponding to the CV-curves in Fig. 2b). The measurements were performed at 800 °C, under OCV conditions.

(two peaks; 1–100 kHz),[21,23,30,31] respectively. The change of the first high-frequency process (1–10 kHz) is mainly attributed to a reduced reaction barrier for the charge transfer process at the triple phase boundary.[30] The slight increase in DRT between 1000 and 100 Hz results from the overlap of the frequency range with the second peak of the Finite-Length Warburg (FLW) diffusion[23,30,32] in the fuel-electrode support and the fuel-electrode electrochemistry. In summary, the higher steam content in the fuel gas results in a lower area-specific resistance (ASR) of the cells due to reduced gas diffusion and charge transfer losses,[20–22] as mentioned above.

I-U performance in r-SOC mode.—Figure 4 shows the performance of SOC-IEK9 and SOC-KIT in r-SOC mode. If it is necessary to convert outside electrical power into chemical power sources, the r-SOCs are in SOEC mode and exhibit -2.0 A cm^{-2}, -0.95 A cm^{-2} and -0.51 A cm^{-2} under 1.2 V at 800 °C, 750 °C and 700 °C, respectively (with respect to practical applications, SOC-IEK9 is discussed here), which means 0.90 l cm^{-2} h^{-1}, 0.43 l cm^{-2} h^{-1} and 0.23 l cm^{-2} h^{-1} of H_2 production (conversion to H_2-volume at room temperature), respectively. The converting performance is not only higher than the published r-SOCs based on the $LaNi_xCo_yFe_{1-x-y}O_3$ system,[14] but is also comparable to the state-of-the-art LSCF-based r-SOCs tested on a laboratory scale.[27,28] If it is necessary to supplement the deficiency of the electrical power, the r-SOCs can be operated in SOFC mode and output current densities of 1.7 A cm^{-2}, 0.92 A cm^{-2} and 0.51 A cm^{-2} under 0.7 V at 800 °C, 750 °C and 700 °C, respectively (SOC-IEK9 is discussed here). As mentioned above, such power output is comparable to the state-of-the-art LSC- based SOFCs and can satisfy commercial requirements. In a laboratory test for SOC-KIT (Fig. 4b), conversion performance (SOEC mode) and power output (SOFC mode) are even higher.

The impedance spectra of SOC-KIT under OCV are also shown in Fig. 5. Similar to the discussion above, the processes of fuel-electrode gas diffusion, air-electrode electrochemistry and fuel-electrode electrochemistry can be distinguished by DRT analysis, where the electrode electrochemistry contributes to the major of ASR, and air-electrode electrochemistry and fuel-electrode electrochemistry contribute almost equally. Compared to the state-of-the-art LSCF-based SOCs, both total ASR values (R_{total}) and their distributions (ohmic resistance R_{ohm} and polarization resistance R_p) are similar to the state-of-the-art LSCF-based SOCs,[23] indicating the similarity of LNC97 and LSCF with respect to the behavior of the air electrode in SOCs.

Mid-term behaviors.—In general, at the current development stages of SOCs, power output or conversion performance are not the key points because in most cases commercial requirements can be satisfied. However, the mid-term stability of SOCs is still a matter of concern because the commercial criterion of 50,000 h operation is hardly reached. Thus, the mid-term stability of SOC-KIT was investigated in detail. In SOEC mode, at 750 °C under 50% H_2O–50% H_2 as fuel gas after 1100 h of operation at -1.0 A cm^{-2}, the voltage degraded from 1.16 V to 1.22 V, which is about 5% (Fig. 4a). However, degradation mainly took place in the first 300 h. If only the stabilized period of the final 800 h is considered, a degradation of 1.6% kh^{-1} is observed. Such degradation is much better than that of the reported SOCs based on $LaNi_xCo_yFe_{1-x-y}O_3$ air electrodes, which is 11.1% kh^{-1}.[14] Even in comparison to the state-of-the-art SOCs based on LSCF air-electrodes (1.9% kh^{-1} as a Ref. 33), such

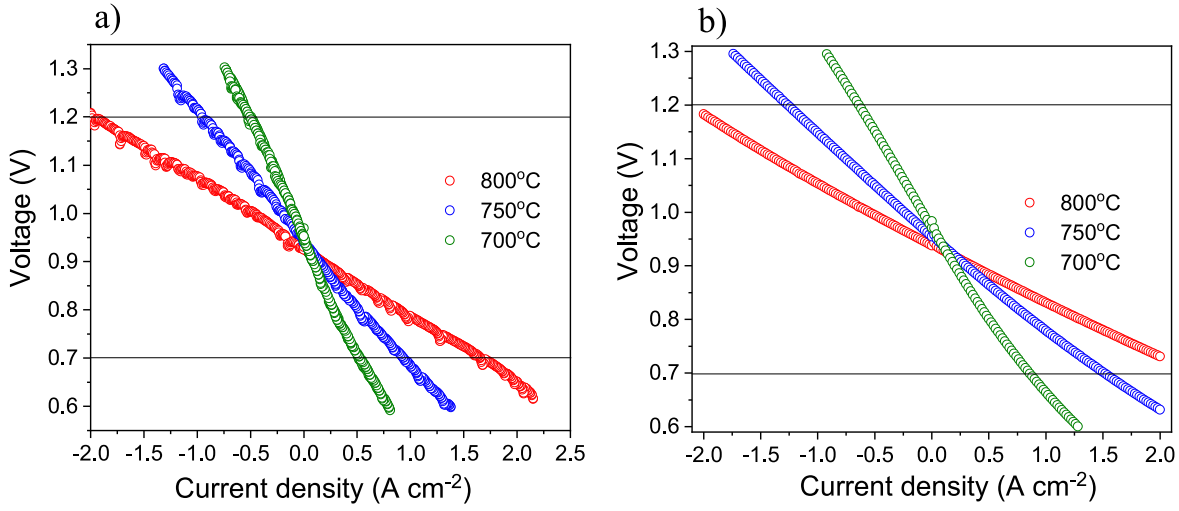

Figure 4. Current–voltage investigations of (a) SOC-IEK9 and (b) SOC-KIT at 700 °C–800 °C in r-SOC mode with 50% H_2O–50% H_2 as fuel gas.

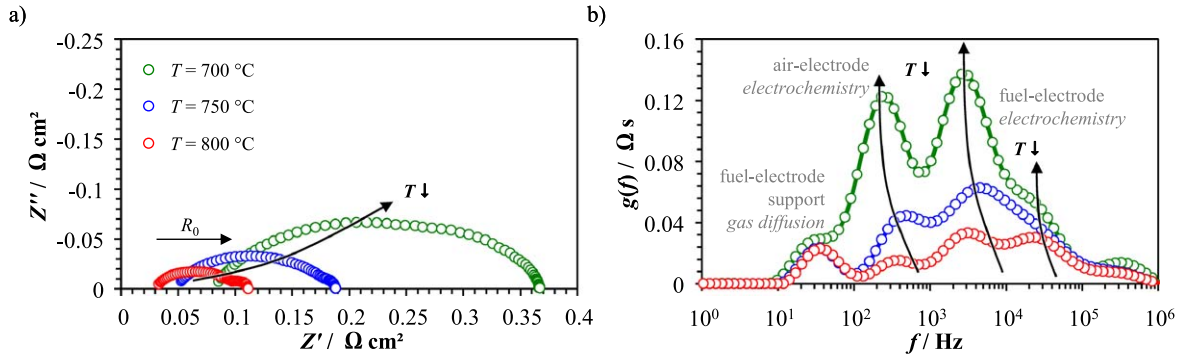

Figure 5. (a) Measured impedance spectra and (b) calculated DRTs for varied temperatures between 700 °C and 800 °C (corresponding to the CV curves in Fig. 4). The measurements were performed under OCV conditions with 50% humidified hydrogen as fuel.

degradation is still comparatively small. Impedance spectra indicate that degradation is mainly caused by polarization (Fig. 6b). In SOFC mode, at 750 °C under 50% H_2O–50% H_2 as fuel gas after 700 h of operation at 1.0 A cm^{-2}, the voltage degraded from 0.77 V to 0.69 V, which is about 10% (Fig. 6b). However, degradation also mainly took place in the first 400 h because of system stabilization. The last 300 h of the test caused no degradation at all. However, a degradation test of around 1000 h is not sufficient to evaluate the situation in practical applications. Nevertheless, these are the longest operating times ever published for $LaCoO_3$–$LaNiO_3$–$LaFeO_3$ air-electrode-based SOCs, providing a very important impression for evaluating these kinds of materials.

Figure 7 shows the temporal evolution of the impedance spectra and DRTs continuously measured during SOEC and SOFC operation. A comparison of the initial impedance spectra shows different polarization behavior for the cell operated in SOFC and SOEC mode although the absolute current density and thus the conversion rate is the same.

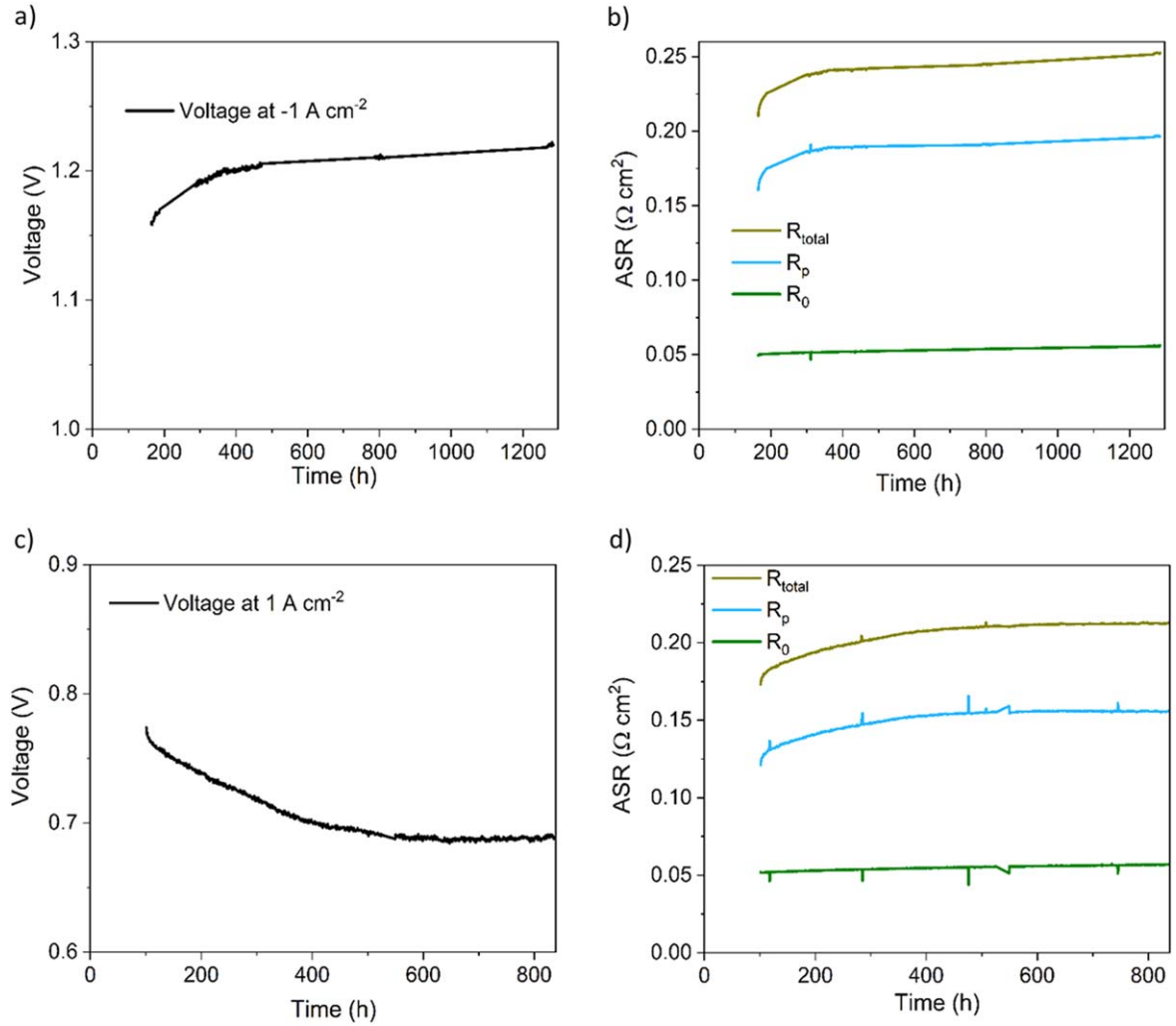

Figure 6. Mid-term stability of SOC-KIT at 750 °C under 50% H_2O–50% H_2 as fuel gas. (a) Voltage degradation at −1.0 A cm^{-2} of a SOC-KIT in SOEC mode. (b) Correlated ASR degradation of the cell in Fig. 6a. (c) Voltage degradation at 1.0 A cm^{-2} of a SOC-KIT in SOFC mode. (d) Correlated ASR degradation of the cell in Fig. 6c.

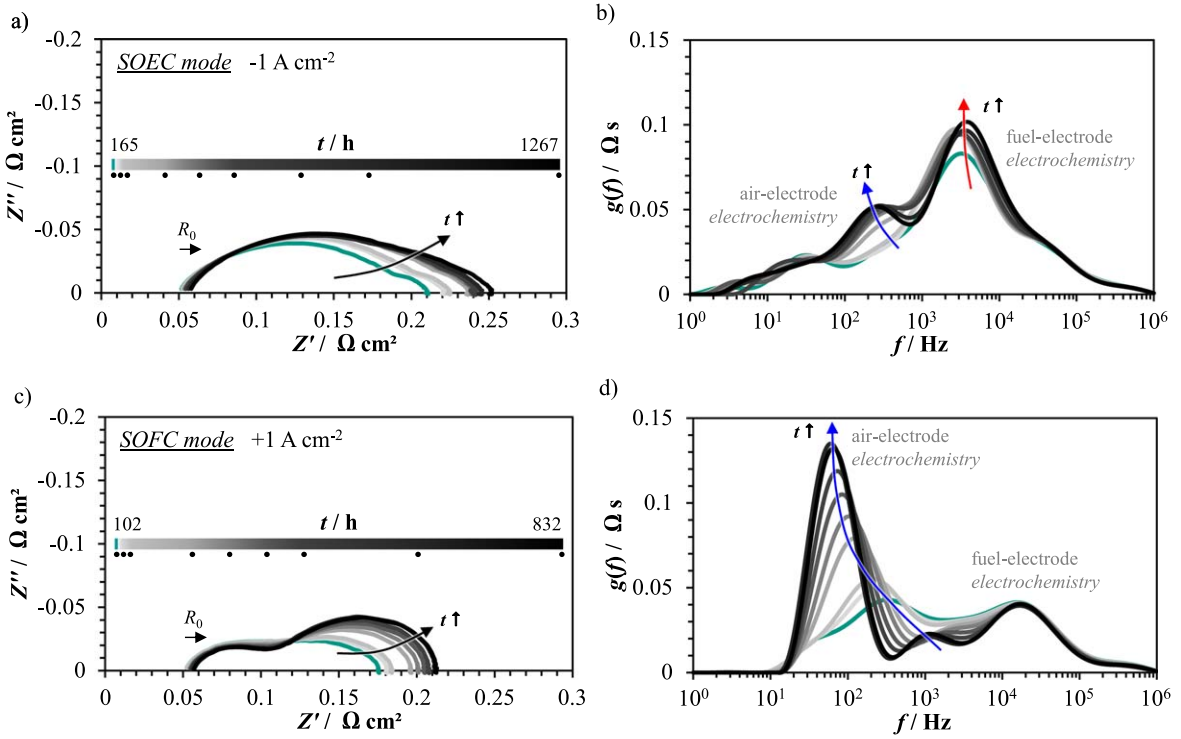

Figure 7. Series of impedance spectra under (a) SOEC and (c) SOFC operation with ±1 A cm^{-2} at 750 °C. All impedance spectra were measured under load. (b) and (d) show the corresponding DRT spectra.

In a direct comparison of both initial spectra, the difference is more evident, as shown in Fig. 8. Thereby, the ohmic resistance of both cells is identical, which confirms the good reproducibility and adhesion of the single cell components. However, the impedance measured in SOEC mode has a 35 mΩ cm^2 higher ASR. According to the DRT analysis in Fig. 8b, the electrochemistry at the fuel-electrode (1 kHz–1 MHz) dominates the ASR in SOEC mode, whereas in SOFC mode the electrochemistry of the air-electrode (1 kHz–1 MHz) has a larger contribution to the ASR. The contribution of the gas diffusion in the fuel-electrode support (1–100 Hz) is similar for both operation modes.

The difference in the contributions of the electrochemical processes of fuel- and air-electrode can be explained by the different reaction directions of the electrochemical oxidation and reduction. In

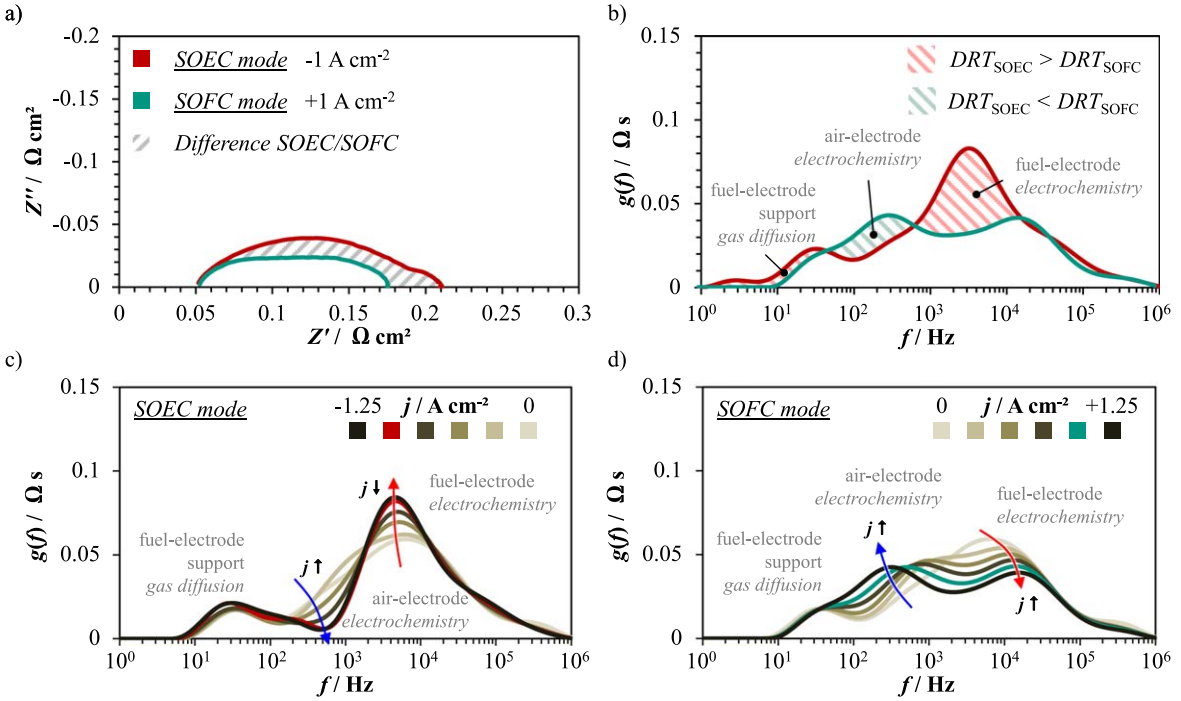

Figure 8. (a) Comparison of the initial impedance spectra under SOEC (165 h) and SOFC operation (102 h) with ±1 A cm^{-2} at 750 °C. All impedance spectra were measured under load. (b) shows the comparison of the corresponding DRT spectra. (c) and (d) show a series of DRTs for varied current densities between ±1.25 A cm^{-2} in 0.25 mA cm^{-2}-steps. The variation was recorded before the aging tests (~70 h) on the cell tested in SOFC mode.

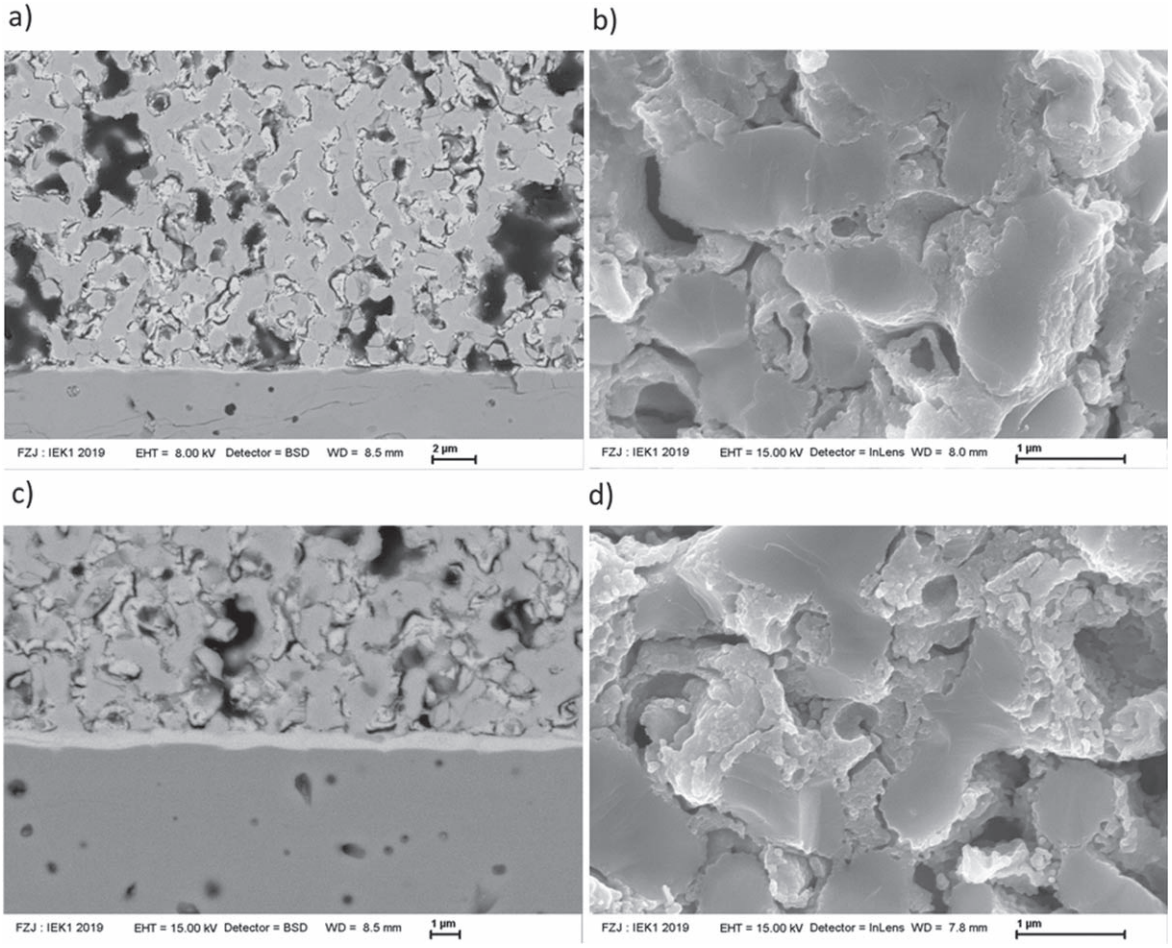

Figure 9. Microstructure of LNC97 based air-electrodes. (a) Polished cross-section after short-term operation of 60 h. (b) Fracture after short-term operation of 60 h. (c) Polished cross-section after mid-term operation of 1200 h. (d) Fracture after mid-term operation of 1200 h.

SOEC operation hydrogen is produced in the fuel-electrode and oxygen is released in the air-electrode, whereas in SOFC operation hydrogen and oxygen are consumed respectively. As a result, the local gas composition in the electrochemically active areas, deviates in SOEC and SOFC mode and leads to different electrode polarizations.

Due to the increasing hydrogen content in SOEC operation the humidification of the fuel is reduced in relative terms. It is known from previous studies on Ni/8YSZ and from the presented results in Fig. 3 that the hydrogen charge transfer reaction is more inhibited for low fuel humidification.[21,23,31] Conversely, the consumption of hydrogen in SOFC operation increases fuel humidification and thus reduces the inhibition of the charge transfer reaction.[21,23,31] Concerning oxygen reduction or evolution, the relation is reversed. In SOFC mode the consumption of oxygen leads to a decrease of the oxygen content, which in turn leads to a stronger inhibition of the oxygen reduction in the air electrode, whereas releasing oxygen in SOEC mode reduces the reaction losses. The same dependency was also observed for LSCF-electrodes.[23,34] The dependence of the gas diffusion for low and high fuel humidification is however almost symmetrical.[23,31,35] To emphasize the discussed dependencies, the Fig. 8c and d depict the different cell behavior for negative (SOEC) and positive (SOFC) current loads. It can be seen that with increasing current, i.e. with a higher conversion rate, the polarization behavior between SOFC and SOFC mode deviates further.

Besides the initial performance, the temporal evolution also differs depending on the operating mode. The DRT analysis in Fig. 7b reveals that in SOEC operation both the electrochemical processes in the fuel- and air-electrode show a slight degradation, whereas in SOFC operation only the air-electrode polarization increases and the fuel-electrode polarization is stable over 800 h (Fig. 7d).

The degradation of the fuel electrode in SOEC mode can be attributed to Ni agglomeration phenomena that are known to be more likely to occur during SOEC operation,[36] while the reason of the degradation in air-electrode is still not clear. Former research analyzed on the temperature programed desorption (TPD) and oxidation (TPO) of LNC97 (pure, no GDC infiltrated), and compared to those of the state-of-the-art LSCF.[8] Although both TPO and TPD of LNC97 are weaker than those of LSCF, the distance of TPD between LNC97 and LSCF is smaller compared to that of TPO, indicating the oxygen reduction reaction is "easier" for LNC97 compared to oxygen oxidation reaction. In other words, the electrochemical balance between Co^{2+} and Co^{3+}, and between Ni^{2+} and Ni^{3+} in LNC97 tends to stay at lower valence compared to that of Co^{2+}/Co^{3+} and Fe^{2+}/Fe^{3+} in LSCF. The reason might be that Ni^{3+} is less stable compared to Fe^{3+} at the operating conditions for LNC97 and LSCF. However, detailed investigation is needed to confirm this point. Nevertheless, the imbalance of LNC97 for oxygen absorption and desorption may be one of the reasons for different electrochemical behavior of the LNC97 based air-electrode under SOEC and SOFC mode.

To further understand the degradation behavior of LNC97-based air electrodes, the microstructures of the electrodes after short- and mid-term operation are compared. In Figs. 9a and 9b, the SOC was operated in SOFC and SOEC mode at 800 °C–650 °C for 60 h. In Figs. 9c and 9d, the SOC was operated in SOFC and SOEC mode at 800 °C–650 °C for 100 h, and was then fixed at 750 °C in SOEC mode of -1 A cm^{-2} with fuel of 50%H_2O–50% H_2 for another

1100 h. The microstructure does not display any obvious difference for either the polished cross section or fracture for LNC97-based electrodes after short- or mid-term operation, indicating the robustness of the electrodes. SEM investigations with energy-dispersive X-ray spectroscopy (EDX) indicate the ideal chemical compatibility of each component in the air electrode and the adjacent part. No apparent element diffusion was found between GDC and LNC97. Although there is a possibility that LNC97 may react with 8YSZ and form $La_2Zr_2O_7$,[8,10] there is no sign of $LaZrO_3$ formation in the 8YSZ electrolyte after 1200 h of SOC operation. In an earlier report by our group,[8] the R_p degradation of LNC97 (5 wt% GDC infiltrated)/GDC symmetric cells was almost 100% after 1000 h of operation at 750 °C and was attributed to the coarsening of infiltrated GDC particles and deterioration of the ionic conduction pathways. In the full cells of the current study, GDC infiltration is increased to 8 wt%. It seems the deterioration problem of the ionic conduction pathways is solved because higher loading of GDC can improve ionic conduction pathways even coarsening should take place. The R_p degradation in this study is only 21% in both SOEC and SOFC mode (Figs. 6b and 6d). However, longer-term testing is still needed to evaluate the material in practical applications and understand the mechanisms behind the degradation phenomenon.

Conclusions

SOCs with dimensions of 5 cm × 5 cm × 0.5 mm were prepared based on conventional NiO-8YSZ fuel-electrode support and functional layer, dense 8YSZ layer, sputtered GDC barrier layer and novel GDC-infiltrated LNC97 air electrode. The power output and conversion performance (in SOFC and SOEC mode, respectively) are not only comparable to state-of-the-art LSCF-based SOFCs but can also satisfy commercial requirements. The mid-term behavior of the cells was investigated for 800 h in SOFC mode and 1100 h in SOEC mode. Degradations are found in both modes, which mainly result from air electrodes in SOFC mode and from both air electrodes and fuel electrodes in SOEC mode. The coarsening of infiltrated GDC particles may be the reason for the degradation of air electrodes. However, longer-term testing is still needed to evaluate the material and electrode.

Acknowledgments

Partial financial support from the KERSOLIFE project, Bundesministerium für Wirtschaft und Energie (BMWi 03ET6101B) is acknowledged. The authors also acknowledge Claudia Tropartz and Tanja Brambach for their valuable help in the electrochemical measurements at IEK-9.

ORCID

Qianli Ma https://orcid.org/0000-0002-4709-4927
Vaibhav Vibhu https://orcid.org/0000-0001-9157-2722
Norbert H. Menzler https://orcid.org/0000-0001-7091-0980

References

1. K. Chen and S. P. Jiang, *J. Electrochem. Soc.*, **163**, F3070 (2016).
2. N. Jordan, W. Assenmacher, S. Uhlenbruck, V. Haanappel, H. Buchkremer, D. Stöver, and W. Mader, *Solid State Ionics*, **179**, 919 (2008).
3. S. Uhlenbruck, T. Moskalewicz, N. Jordan, H.-J. Penkalla, and H. Buchkremer, *Solid State Ionics*, **180**, 418 (2009).
4. E. Konysheva, H. Penkalla, E. Wessel, J. Mertens, U. Seeling, L. Singheiser, and K. Hilpert, *J. Electrochem. Soc.*, **153**, A765 (2006).
5. K. Kendall and M. Kendall, *High-Temperature Solid Oxide Fuel Cells for the 21st Century: Fundamentals, Design and Applications* (Elsevier, London) (2015).
6. H. Orui, K. Watanabe, R. Chiba, and M. Arakawa, *J. Electrochem. Soc.*, **151**, A1412 (2004).
7. F. Tietz, I. A. Raj, Q. Ma, S. Baumann, A. Mahmoud, and R. Hermann, *J. Solid State Chem.*, **237**, 183 (2016).
8. Q. Ma, M. Balaguer, D. Pérez-Coll, L. G. de Haart, J. M. Serra, G. C. Mather, F. Tietz, N. H. Menzler, and O. Guillon, *ACS Appl. Energy Mater.*, **1**, 2784 (2018).
9. R. Chiba, F. Yoshimura, and Y. Sakurai, *Solid State Ionics*, **124**, 281 (1999).
10. T. Komatsu, R. Chiba, H. Arai, and K. Sato, *J. Power Sources*, **176**, 132 (2008).
11. T. Komatsu, K. Watanabe, M. Arakawa, and H. Arai, *J. Power Sources*, **193**, 585 (2009).
12. P. Hjalmarsson and M. Mogensen, *J. Power Sources*, **196**, 7237 (2011).
13. B. Huang, X.-J. Zhu, H.-W. Nie, Y.-R. Niu, Y. Li, and N. Cheng, *J. Power Sources*, **235**, 20 (2013).
14. A. Chrzan, S. Ovtar, P. Jasinski, M. Chen, and A. Hauch, *J. Power Sources*, **353**, 67 (2017).
15. Y. Li, J. Cai, J. A. Alonso, H. Lian, X. Cui, and J. B. Goodenough, *Int. J. Hydrogen Energy*, **42**, 27334 (2017).
16. M. Pechini, *Method of preparing lead and alkaline earth titanates and niobates and coating method using the same to form a capacitor*, U.S.A. Pat. No. 3330697 (1967).
17. M. Schönleber, D. Klotz, and E. Ivers-Tiffée, *Electrochim. Acta*, **131**, 20 (2014).
18. H. Schichlein, A. C. Müller, M. Voigts, A. Krügel, and E. Ivers-Tiffée, *J. Appl. Electrochem.*, **32**, 875 (2002).
19. E. Ivers-Tiffee and A. Weber, *J. Ceram. Soc. Jpn.*, **125**, 193 (2017).
20. J. Mizusaki, H. Tagawa, T. Saito, T. Yamamura, K. Kamitani, K. Hirano, S. Ehara, T. Takagi, T. Hikita, and M. Ippommatsu, *Solid State Ionics*, **70**, 52 (1994).
21. A. Utz, H. Störmer, A. Leonide, A. Weber, and E. Ivers-Tiffée, *J. Electrochem. Soc.*, **157**, B920 (2010).
22. Q. Ma, F. Tietz, A. Leonide, and E. Ivers-Tiffée, *ECS Trans.*, **35**, 1421 (2011) 10.1149/1.3570128.
23. A. Leonide, V. Sonn, A. Weber, and E. Ivers-Tiffée, *J. Electrochem. Soc.*, **155**, B36 (2007).
24. D. Klotz, A. Weber, and E. Ivers-Tiffée, *Electrochim. Acta*, **227**, 110 (2017).
25. F. Han, R. Mücke, T. Van Gestel, A. Leonide, N. H. Menzler, H. P. Buchkremer, and D. Stöver, *J. Power Sources*, **218**, 157 (2012).
26. S. Uhlenbruck, N. Jordan, D. Sebold, H. Buchkremer, V. Haanappel, and D. Stöver, *Thin Solid Films*, **515**, 4053 (2007).
27. D. Klotz, A. Leonide, A. Weber, and E. Ivers-Tiffée, *Int. J. Hydrogen Energy*, **39**, 20844 (2014).
28. J.-C. Njodzefon, D. Klotz, A. Kromp, A. Weber, and E. Ivers-Tiffée, *J. Electrochem. Soc.*, **160**, F313 (2013).
29. Y. Yan, Q. Fang, L. Blum, and W. Lehnert, *Electrochim. Acta*, **258**, 1254 (2017).
30. S. Dierickx, T. Mundloch, A. Weber, and E. Ivers-Tiffée, *J. Power Sources*, **415**, 69 (2019).
31. S. Dierickx, J. Joos, A. Weber, and E. Ivers-Tiffée, *Electrochim. Acta*, **265**, 736 (2018).
32. J. Bisquert and A. Compte, *J. Electroanal. Chem.*, **499**, 112 (2001).
33. M. Al Daroukh, F. Tietz, D. Sebold, and H. Buchkremer, *Ionics*, **21**, 1039 (2015).
34. C. Endler, A. Leonide, A. Weber, F. Tietz, and E. Ivers-Tiffée, *J. Electrochem. Soc.*, **157**, B292 (2010).
35. S. Primdahl and M. Mogensen, *J. Electrochem. Soc.*, **146**, 2827 (1999).
36. Q. Fang, C. E. Frey, N. H. Menzler, and L. Blum, *J. Electrochem. Soc.*, **165**, F38 (2018).